SCIENCE ADVANCES | RESEARCH ARTICLE

Submitted 16 August 2016
Accepted 10 February 2017
Published 5 April 2017
10.1126/sciadv.1601939

APPLIED SCIENCES AND ENGINEERING

Design and function of biomimetic multilayer water purification membranes

Shengjie Ling,[1,2]* Zhao Qin,[1]* Wenwen Huang,[2] Sufeng Cao,[3] David L. Kaplan,[2]† Markus J. Buehler[1,4,5]†

[1]Department of Civil and Environmental Engineering, Massachusetts Institute of Technology, 77 Massachusetts Avenue, Cambridge, MA 02139, USA.

[2]Department of Biomedical Engineering, Tufts University, Medford, MA 02155, USA.

[3]Department of Chemical and Biological Engineering, Tufts University, Medford, MA 02155, USA.

[4]Center for Materials Science and Engineering, Massachusetts Institute of Technology, Cambridge, MA 02139, USA.

[5]Center for Computational Engineering, Massachusetts Institute of Technology, Cambridge, MA 02139, USA.

*These authors contributed equally to this work.

Anil Kumar A
21 July 2018

Background work and relevant to the lab

analytical chemistry

Letter

dx.doi.org/10.1021/ac502779r | *Anal. Chem.* 2014, 86, 10996−11001 pubs.acs.org/ac

Approaching Sensitivity of Tens of Ions Using Atomically Precise Cluster−Nanofiber Composites

Atanu Ghosh,[†] Vedhakkani Jeseentharani,[†] Mohd Azhardin Ganayee,[†] Rani Gopalakrishnan Hemalatha,[†] Kamalesh Chaudhari,[†] Cherianath Vijayan,[‡] and Thalappil Pradeep*[,†]

[†]DST Unit of Nanoscience (DST UNS) and Thematic Unit of Excellence (TUE), Department of Chemistry, Indian Institute of Technology Madras, Chennai 600 036, India

[‡]Department of Physics, Indian Institute of Technology Madras, Chennai 600 036, India

analytical chemistry

Article

pubs.acs.org/ac

DOI: 10.1021/acs.analchem.5b04520
Anal. Chem. 2016, 88, 5710−5717

Electrospun Nanofiber Mats as "Smart Surfaces" for Desorption Electrospray Ionization Mass Spectrometry (DESI MS)-Based Analysis and Imprint Imaging

R. G. Hemalatha, Mohd Azhardin Ganayee, and T. Pradeep*

DST Unit on Nanoscience and Thematic Unit of Excellence, Department of Chemistry, Indian Institute of Technology Madras, Chennai 600 036, India

ACS Sustainable Chemistry & Engineering

Research Article

Cite This: ACS Sustainable Chem. Eng. 2018, 6, 2942−2953

pubs.acs.org/journal/ascecg

Poly(ether sulfone) Nanofibers Impregnated with β-Cyclodextrin for Increased Micropollutant Removal from Water

Andrea I. Schäfer,[†] Katharina Stelzl,[†,‡] Maryam Faghih,[†] Soujit Sen Gupta,[‡] Kumaranchira Ramankutty Krishnadas,[‡] Stefan Heißler,[§] and Thalappil Pradeep*[,‡]

[†]Membrane Technology Department, Institute of Functional Interfaces (IFG), Karlsruhe Institute of Technology (KIT), Hermann-von-Helmholtz-Platz 1, 76344 Eggenstein-Leopoldshafen, Germany

[‡]DST Unit of Nanoscience (DST UNS) and Thematic Unit of Excellence (TUE), Department of Chemistry, Indian Institute of Technology Madras, Chennai 600 036, India

[§]Chemistry of Oxydic and Organic Interfaces Department, Institute of Functional Interfaces (IFG), Karlsruhe Institute of Technology (KIT), Hermann-von-Helmholtz-Platz 1, 76344 Eggenstein-Leopoldshafen, Germany

Introduction

- Membranes for water treatment have progressively been developed in recent years to address global challenges of water pollution, because they are an energy- and waste-efficient means to remove molecular level contaminant.

- Multilayer architectures in water purification membranes enable **increased water throughput, high filter efficiency, and high molecular loading capacity.**
- However, the preparation of membranes with well-organized multilayer structures, starting from the nanoscale to maximize filtration efficiency, remains a challenge.
- The main objective is to prepare **low-cost water purification membranes while retaining mechanical strength and high purification performance.**
- Nature has used multilayer architectures for water purification for millions of years in environments that consist of vegetation, gravel, sand, and soil layers.

- **The challenge is to directly mimicking the design and ingenuity of nature in the laboratory for practical applications.**

Continued….

- However, it remains a challenge to efficiently and accurately produce multilayer porous structures of biomaterials. This limitation is due to the challenges of materials design, which require an **in-depth understanding of both the molecular interactions and chemical processes.**

- Many natural systems, such as nacre, enamel, and bone, **use proteins and calcium-based minerals** to build their sophisticated multilayer architectures with enhanced physical properties.

- Moreover, both proteins and calcium-based minerals have shown promising applications in water purification and other extensive fields; thus, **the authors selected these two components as starting building blocks to generate the composites.**

Liquid-exfoliated silk nanofibrils (SNFs) used to make filtration membranes with high water flux and efficient separation performance for dyes, proteins, and nanoparticles (Ling et al., Ultrathin free-standing Bombyx mori silk nanofibril membranes. *Nano Lett. 16, 3795–3800* **(2016).**

Results and Discussion

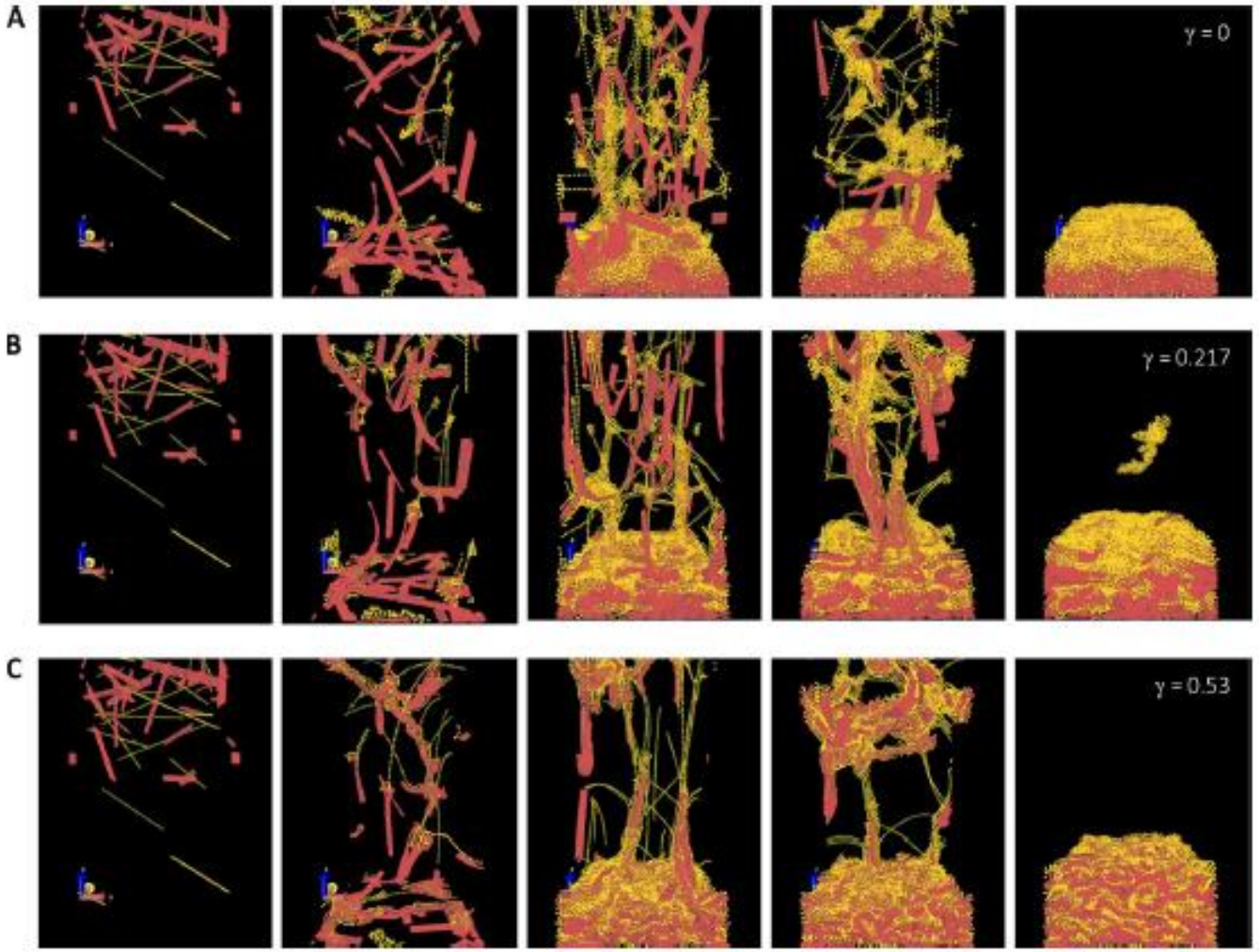

Figure 1. Coarse-grained computational MD simulations of SNF/HAP assembly and deposition. Elastic network models are built on mechanics and geometry feature of the unit building blocks. HAP-SNF surface energy g (J/m2) is not certain because it depends on the molecular structure and the hierarchy structure of the interface in contact. This is important in forming the layered structure. For the SNF/HAP model, HAP and SNF particles were randomly distributed initially and then subjected to a gravity field that accounts for the drag force from the water flow. (A to C) Snapshots of the HAP/SNF assembly process during deposition, with g set as 0 (A), 0.217 J/m^2 (B), and 0.53 J/m^2 (C).

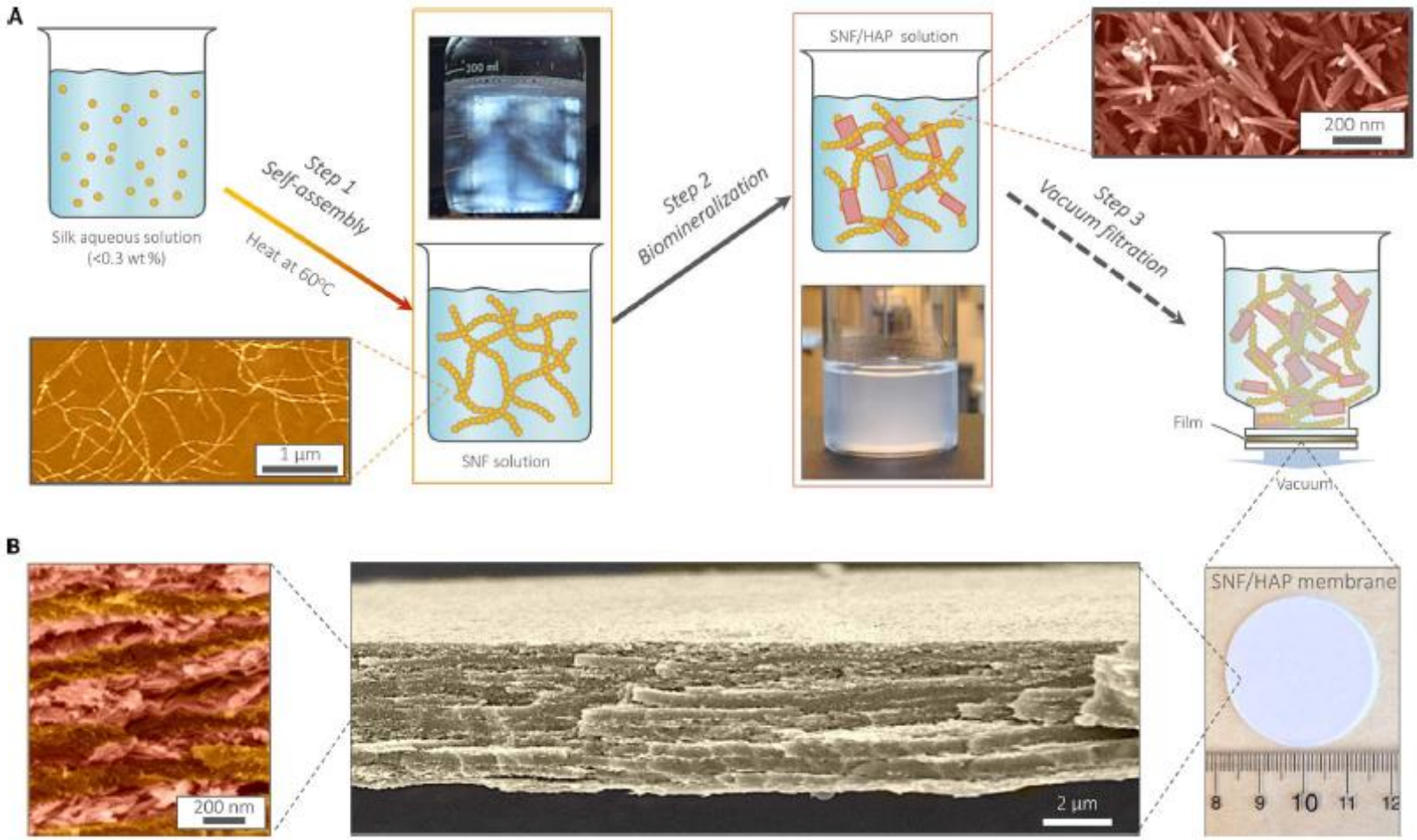

Figure 2. The pathway to fabricate the SNF/HAP membranes and visualization of typical multilayer structures formed. (A) Schematic of the preparation steps of SNF/HAP membranes. Step 1: Silk was assembled to SNFs in aqueous solution. The bottom image in the first row is an atomic force microscopy (AFM) image of SNFs; the top image in the second row is the SNF solution under polarized light, indicating the presence of a nematic phase of SNFs. Step 2: The SNFs were used as templates to induce the growth of HAP nanocrystals. The bottom image in the third row is an image of SNF/HAP solution; the top image in the fourth row is a scanning electron microscopy (SEM) image of biomineralized HAP nanocrystals. Step 3: SNF/HAP dispersions were assembled into membranes via vacuum filtration. (B) Multilayer structures of the membranes. The third image is an SNF/HAP membrane with a thickness of 4 mm. This membrane was directly moved from the supporting substrate after filtration of the SNF/HAP dispersion in a process that took 9 s. The second image is the cross-sectional SEM image of SNF/HAP membrane, which shows nacre-like, highly ordered multilayer structures. The first image is the high-resolution cross-sectional SEM of an SNF/HAP membrane. The clear SNF- and HAP-rich layers can be observed. False color was used in AFM and SEM images.

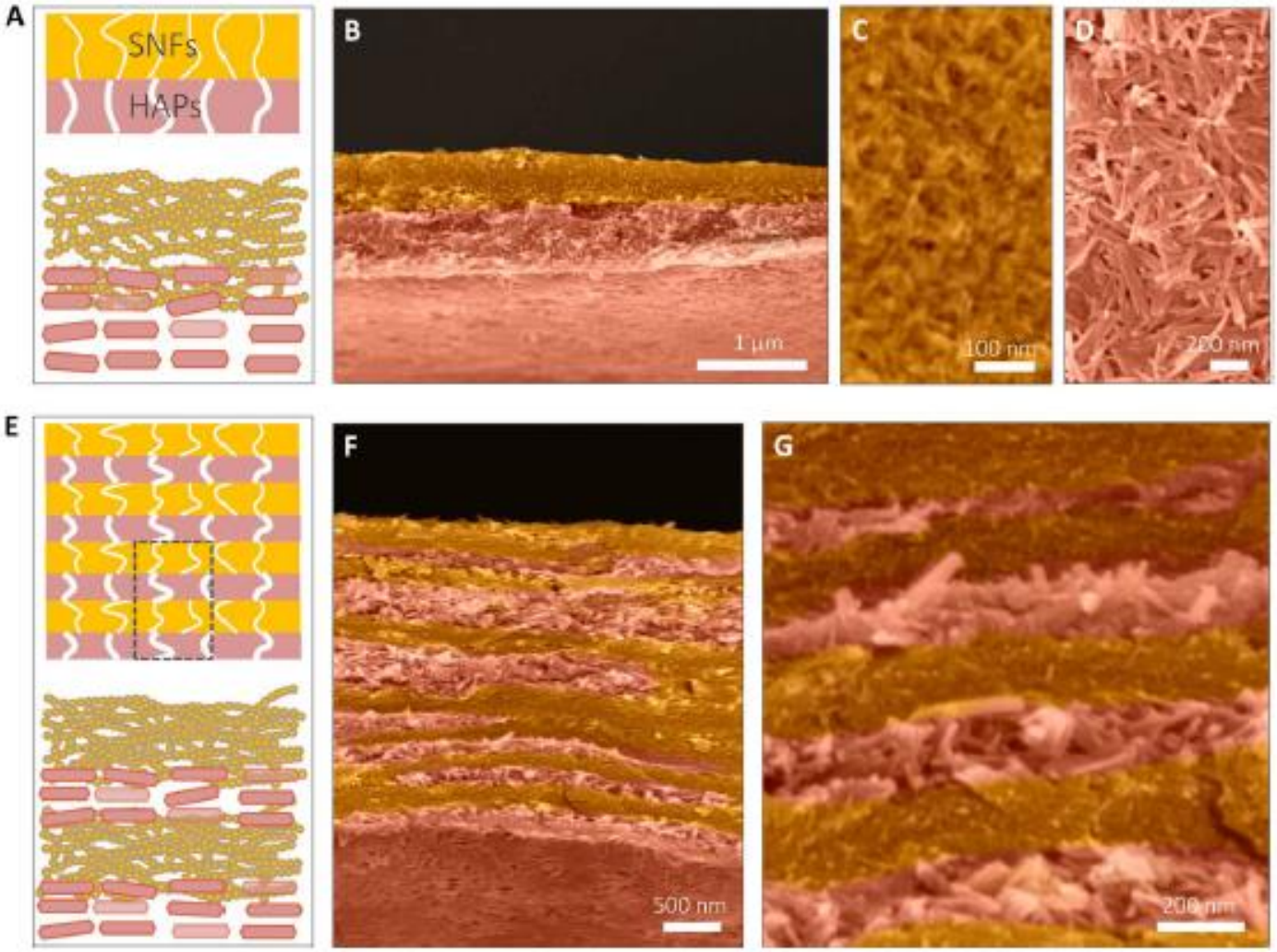

Figure 3. The well-organized multilayer structures of SNF/HAP membranes. (A to D) The double-layer structure of the SNF/HAP membranes was formed through vacuum filtration of 1 ml of dispersion. (A) Schematic of double-layer structures. The top layer is the SNF-rich layer with small pore sizes. The bottom layer is the HAP layer with larger pore sizes. (B) Cross-sectional SEM image of a double-layer membrane. (C and D) Top-view SEM images of SNF-rich (C) and HAP-rich (D) layers. (E to G) The multilayer structure of the SNF/HAP membrane was generated from 3-ml SNF/HAP dispersion using a 3.5-cm-diameter mold. (E) Schematic of multilayer structures. (F) Cross sectional SEM image of a multilayer membrane. (G) High-resolution cross-sectional SEM image of a multilayer membrane. False color is used in SEM images.

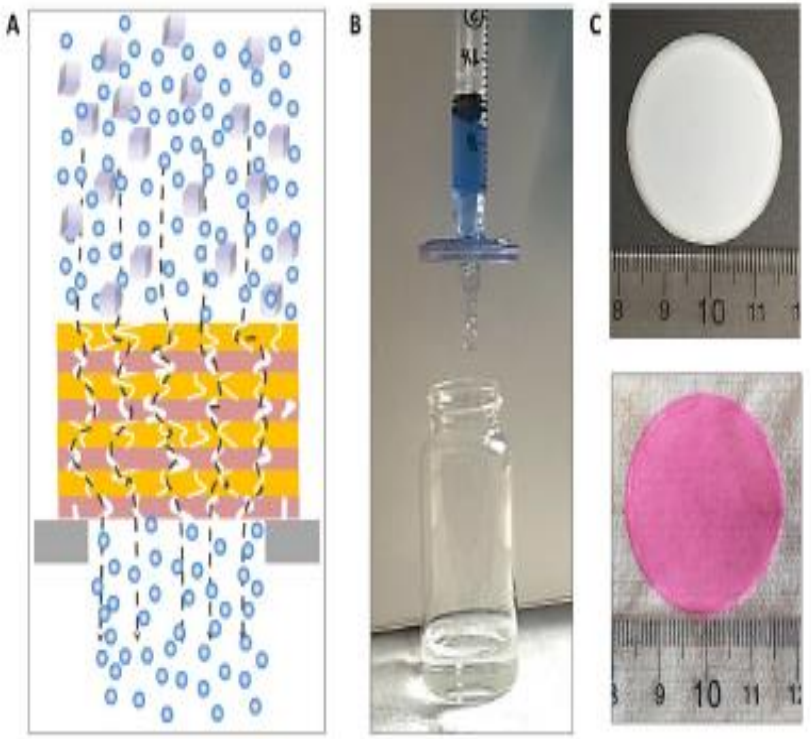

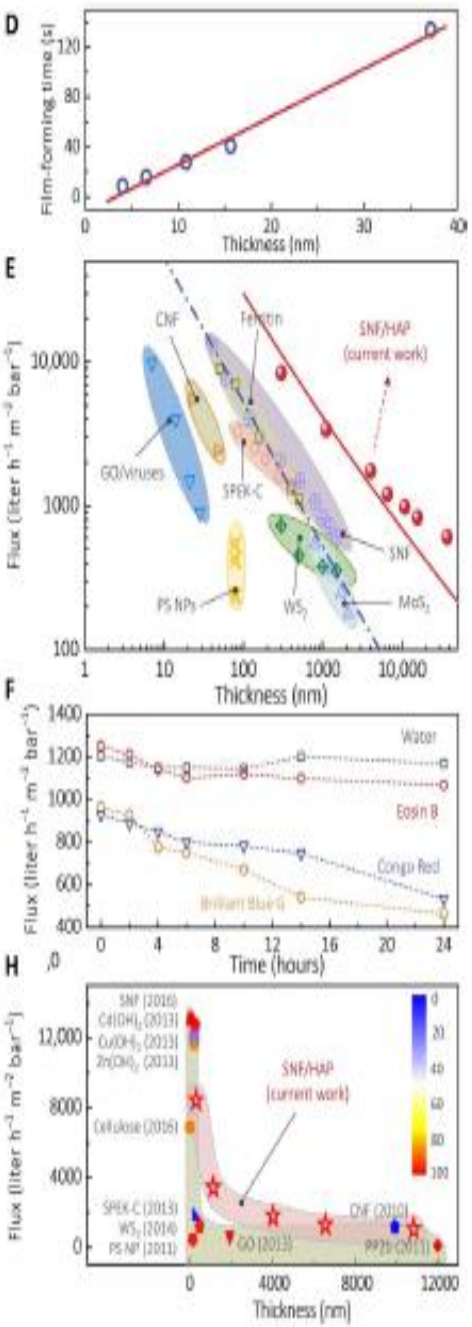

G Separation performance of 7-μm-thick SNF/HAP membranes for model compounds.

	Concentration	Flux (liter h^{-1} m^{-2} bar^{-1})	Rejection at 10 min (%)	Rejection at 2 hours (%)	Rejection at 24 hours (%)
Green fluorescent protein	0.05 mg ml^{-1}	1079.4	91.1	92.6	-
Cytochrome c	2.0 mg ml^{-1}	1253.6	97.8	61.8	-
Bovine serum albumin	2.0 mg ml^{-1}	635.9	70.2	33.3	10.7
Gold nanoparticles	~5.5×10^{13} unit per ml	1185.4	100	100.0	-
Eosin B	251 μM	1287.6	64.9	57.0	13.5
Orange G	306 μM	1015.4	76.7	32.1	18.7
Alcian Blue 8GX	80 μM	881.4	100	100	100
Brilliant Blue G	139 μM	927.9	100	100	100
Brilliant Blue R-250	44 μM	686.8	100	99.8	99.8
Alizarin Red S	434 μM	819.1	99.3	91.1	88.8
Rhodamine B	171 μM	1106.8	100	49.3	40.8
Congo Red	153 μM	964.8	100	100.0	90.9
Direct Red 81	240 μM	1019.7	99.8	88.3	56.4
Fluorescent Brightener 28	85 μM	1145.0	100	93.7	92.2

Figure 4. Separation performance of SNF/HAP membranes. (A) Cross-sectional representation of a multilayer SNF/HAP membrane to filter compounds. (B) Image of the SNF/HAP-based syringe nanofilter, which successfully rejected Alcian Blue 8GX with a rejection of 98%. The detailed structures of SNF/HAP membranes formed on microfilters can be found in fig. S16B. (C) SNF/HAP nanofiltration membrane before (top) and after (bottom) filtration with 20 ml of 5 mM Rhodamine B solution. (D) Linear relationship between film thickness and film formation processing time. (E) Thickness-dependent changes in permeability to pure water for the SNF/HAP membranes and other previously reported membranes. The blue dash-dot line is a fitted curve using the Hagen-Poiseuille equation with uniform structure. The red solid line is a fitted curve using Eq. 1 for multilayer membrane (see also section S8). (F) Time-dependent changes in the flux of water and dye solution within 24 hours of flow. (G) Separation performance of 7-mm-thick SNF/HAP membranes for dyes, proteins, and colloids after 10 min, 2 hours, and 24 hours of flow. The flux listed in the table was calculated from the filtration of model compound solutions. The filtration pressure was kept at 80 kPa in all these tests. Several dye solutions have lower flux than pure water, likely because of their large molecular size, which would be responsible for blocking the pores of membranes. (H) Comparison of the 5-nm gold nanoparticle separation performance of SNF/HAP membranes to that of other filtration membrane materials. The rejection is represented by the color of the pattern. The blue and red are 0 and 100% rejection, respectively.

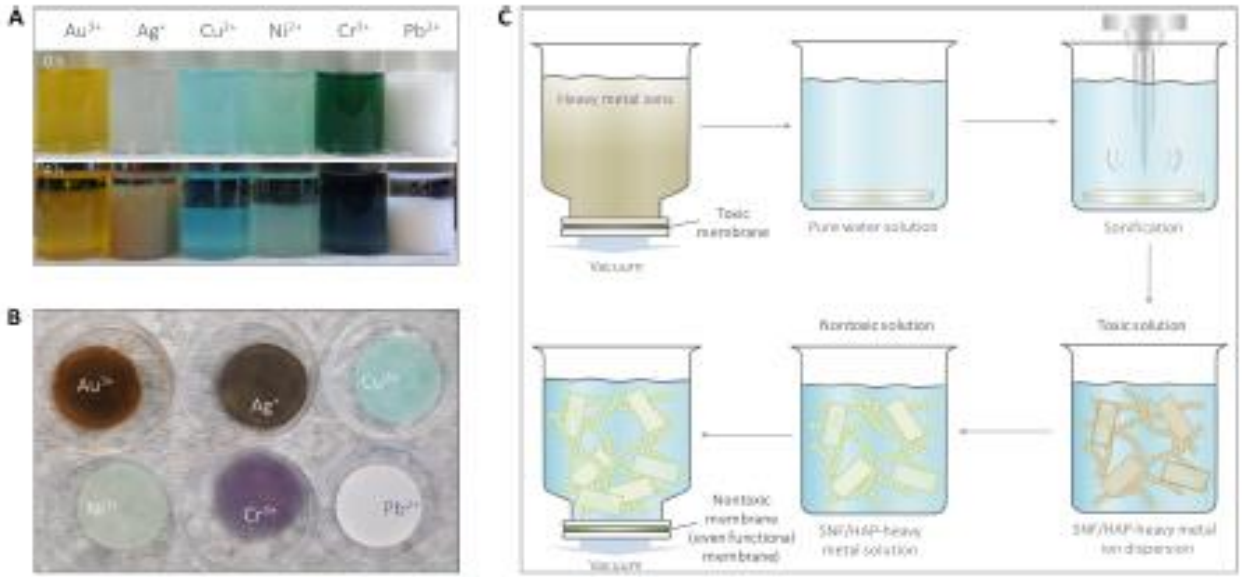

D

Separation and adsorption performance of SNF/HAP nanocomposites for heavy metal ions.

	IARC classification	Guideline for drinking water quality (mg/l)	Removing capacity of membrane (mg/g)	Maximum adsorption capacity (mg/g)	Postprocessing method	The materials prepared from postprocessing	Potential recycle application
Au^{3+}	–	–	135.7	164.2	Illumination	Gold nanosheets	Electronics
					Hydrothermal	Gold nanoparticles	Catalyst
Ag^{+}	–	–	–	–	Illumination	Ag nanoparticles	Antibacterium
Cu^{2+}	–	2	64.7	136.8	$NaBH_4$ reducing	Cu nanoparticles	Electronics
					Adding NaOH	CuO nanocrystals	Electrode
Ni^{2+}	Group 1	0.07	63.0	132.5	$NaBH_4$ reducing	Ni nanocrystals	Magnetic
Cr^{3+}	Group 3	0.05	126.7	145.8	Adding NaOH	Cr_2O_3	Pigment
Pb^{2+}	Group 2A	0.07	–	–	Reaction with H_2S gas	PbS nanoparticles	Catalyst

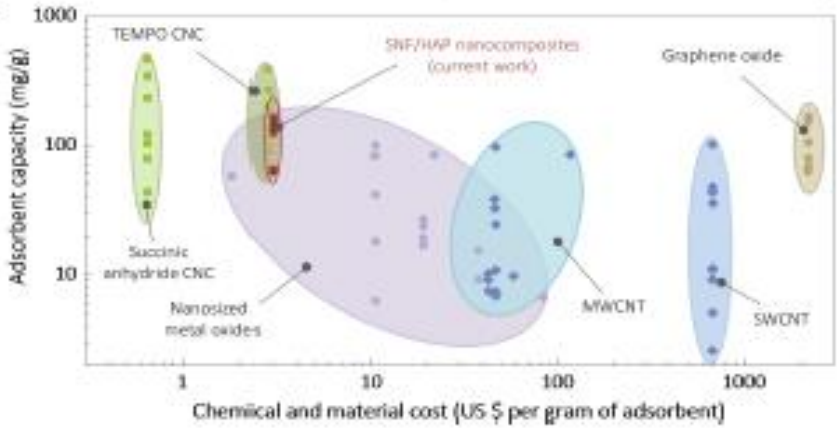

Figure 5. Removal and recycling of heavy metal ions by SNF/HAP membranes. (A) Image of SNF/HAP dispersion-adsorbed metal ions at 0 and 24 hours (see section S10 for more details). (B) Image of an SNF/HAP membrane after metal ions were adsorbed through flux-controllable filtration. (C) Schematic of a general route for recycling metal ion contaminants by redispersion of saturated SNF/HAP membrane (see section S11 for more details). (D) Table of separation and adsorption performance of SNF/HAP nanocomposites for heavy metal ions (see section S10 for more details). The adsorbent capacity of Ag^{+} and Pb^{2+} is not listed quantitatively because Ag^{+} and Pb^{2+} interacted with Cl^{-} to yield a precipitate. The maximum adsorption capabilities of SNF/HAP composite for metal ions were calculated from equilibrium adsorption isotherms data (see section S10 for details). IARC, International Agency for Research on Cancer. (E) Gold contaminants can be reused after facile and green postprocessing (see section S11 for more details about postprocessing for metal ions). (F) Cost and adsorption capacity estimates for the most-studied nanomaterials. The detailed calculations and comparisons of these materials are shown in section S12. TEMPO, 2,2,6,6-tetramethylpiperidine 1-oxyl; MWCNT, multiwalled carbon nanotube; SWCNT, single-walled carbon nanotube.

Equations used for the data interpretation

- The total energy of each SNF/HAP unit is given by $E = E_T + E_B + E_{nonbond}$

  where E_T is the tensile deformation energy for fiber stretching, E_B is for bending, and $E_{nonbond}$ is for nonbonded interaction with other SNF and HAP beads.

- The drag force was given by the Stokes' law as $f_{drag} = -6\pi\mu Rv$

  where R is the effective bead radius for SNF and HAP materials, μ = 8.6 × 10−4 Pa.s is the fluid viscosity constant of water at room temperature, and v = 250 m/s is the flow velocity.

- Starting from the Hagen-Poiseuille equation, the water flux of the SNF/HAP multilayer membrane was derived and given by $f_{flux} = \frac{\pi(h_1 + h_2)}{8\mu H\left(\frac{h_1}{\beta_1 r_2^4} + \frac{h_2}{\beta_2 r_2^4}\right)}$

  where H is the total thickness, m is the viscosity of water, and h_i and r_i are the average thickness and the average radius of the pores, respectively, with lower index 1 for the SNF layer and lower index 2 for the HAP layer. β_i accounts for the pore's surface density and shape factor.

- Rejection (R; %) was calculated by $R = \left(1 - \frac{C_p}{C_f}\right) \times 100\%$

  where C_f and C_p are the concentrations of the compounds in the feed and permeate, respectively.

Conclusions

- The authors reported a new and optimized biomimetic route to fabricate biomaterial-based multilayer membranes for water purification consisting of **well-organized multilayer structures** through silk self-assembly and in situ HAP biomineralization.

- Exhibiting universal water purification capability for **dyes, proteins, and nanocolloids.**
- The SNF/HAP composites show optimum performance in terms of both price and adsorbent capacity and they are **much more effective** for water treatment than CNC hydrogels.

- The cost of SNF/HAP membrane is approximately **$3.36 per gram,** which is comparable with that of cellulose nanocrystal (CNC) materials **($0.65 to $2.80).**

- Fabrication of multitype purification membranes, such as pressure-derived filtration membranes and syringe ultrafilters **are possible with this approach.**

- **Useful application in wastewater treatment, nanotechnology, food industry, and the life sciences.**

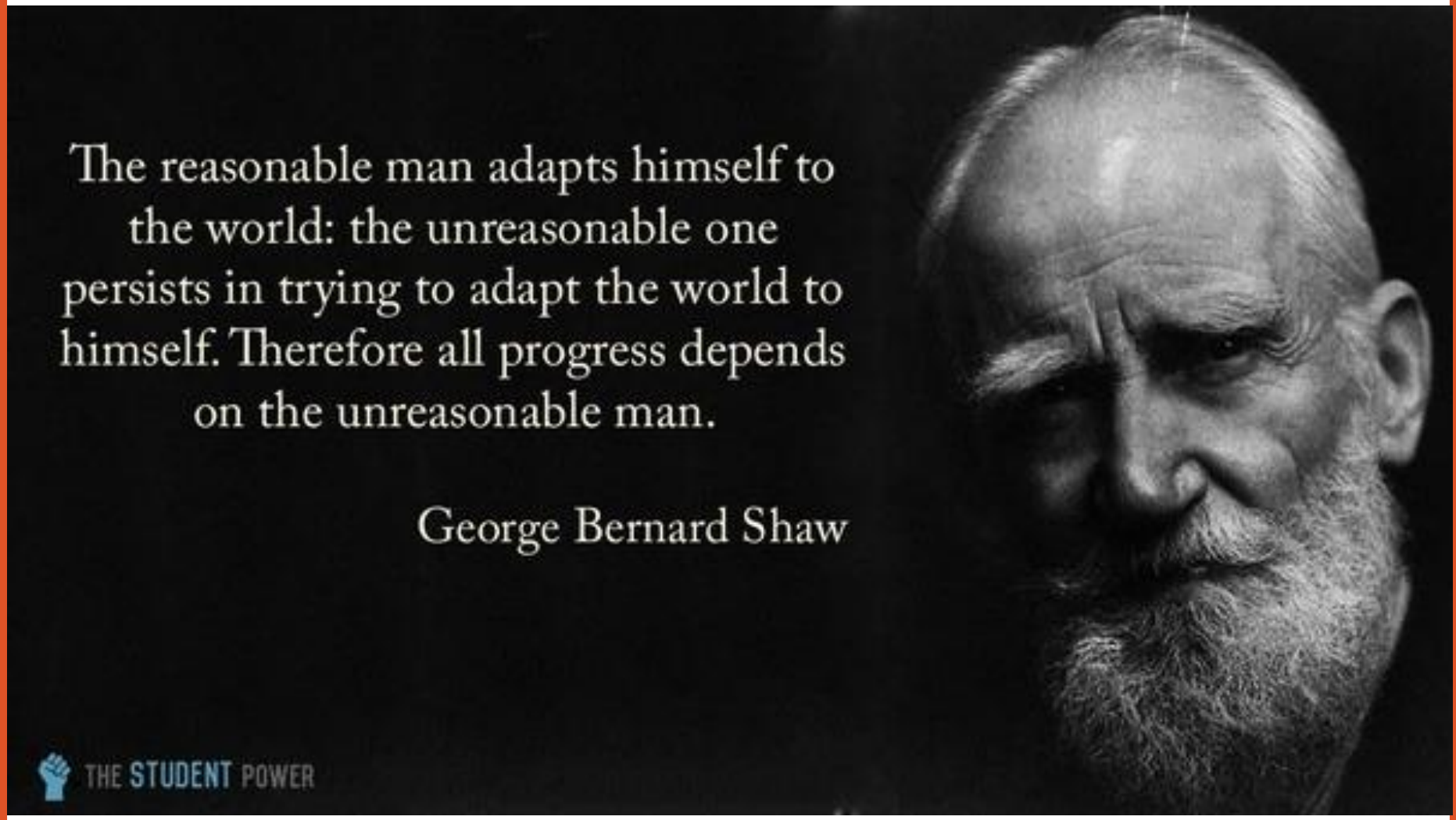
The reasonable man adapts himself to the world: the unreasonable one persists in trying to adapt the world to himself. Therefore all progress depends on the unreasonable man.
George Bernard Shaw
THE STUDENT POWER